Gain Normalized Adaptive Observer For Three-Phase System

Ahmed, H., Pay, M. L., Benbouzid, M., Amirat, Y. & Elbouchikhi, E.

Original citation & hyperlink:
Ahmed, H, Pay, ML, Benbouzid, M, Amirat, Y & Elbouchikhi, E 2020, 'Gain Normalized Adaptive Observer For Three-Phase System' International Journal of Electrical Power and Energy Systems, vol. 118, 105821.
https://dx.doi.org/10.1016/j.ijepes.2020.105821

DOI 10.1016/j.ijepes.2020.105821
ISSN 0142-0615

Publisher: Elsevier

Gain Normalized Adaptive Observer For Three-Phase System

Hafiz Ahmed[a,*], Miao Lin Pay[b], Mohamed Benbouzid[c,e], Yassine Amirat[d], Elhoussin Elbouchikhi[d]

[a] *School of Mechanical, Aerospace and Automotive Engineering, Coventry University, Coventry CV1 5FB, United Kingdom.*
[b] *School of Engineering and Technology, University of Hertfordshire, Hatfield, AL10 9AB, United Kingdom.*
[c] *University of Brest, UMR CNRS 6027 IRDL, 29238 Brest, France.*
[d] *ISEN Brest, Yncréa Ouest, UMR CNRS 6027 IRDL, 29200 Brest, France.*
[e] *Shanghai Maritime University, 201306 Shanghai, China.*

Abstract

This paper proposes the estimation of parameters and symmetrical components of unbalanced grid using adaptive observer framework. Recent adaptive observers proposed in the literature doesn't employ any gain normalization in their frequency estimation loop. This can be problematic in the presence of large voltage dip. This paper proposes a solution to overcome this limitation using a novel gain normalized - frequency-locked loop (GN-FLL). Technical details of GN-FLL, stability analysis and tuning are provided in this paper. Comparative experimental results with adaptive Luenberger observer, second-order generalized integrator - phase-locked loop (SOGI-PLL) and enhanced PLL (EPLL) are provided to demonstrate the effectiveness the proposed technique in the single-phase case. Comparative experimental results with double SOGI-FLL (DSOGI-FLL) and adaptive notch filter (ANF) are provided to demonstrate the effectiveness the proposed technique in the three-phase case.

Keywords: Frequency-Locked Loop (FLL), Three-Phase Sequence Detection, Phase Estimation, Frequency Estimation

1. Introduction

In the control, synchronization and monitoring of grid-connected power converters, parameters of the grid voltage specially phase, frequency, symmetric components etc. play a very important role [1, 2]. This is a challenging topic specially in the context of increased renewable energy penetration in the traditionally unidirectional power grid.

In the context of grid integration of renewable energy sources, grid synchronization plays a vital role. There are many types of grid synchronization algorithms. Among them, grid synchronizing current controller is a popular technique for both single-phase and three-phase systems [3, 4]. In the single-phase case, to generate the reference current, the knowledge of instantaneous phase of the grid voltage signal is required. In the three-phase case, in addition to the instantaneous phase, sequence components are also required to control the power flow for unbalanced grid. As a result, accurate estimation of grid voltage parameters can be considered as a vital element of grid synchronization algorithm. This has led to numerous results on this topic in the literature.

There are several results available in the literature on the parameter estimation of grid voltage signal. The types of techniques that are proposed use a wide variety of methods. Some of the techniques are: open or pseud open-loop technique [5], frequency domain methods (e.g. discrete Fourier transform [6]), maximum-likelihood estimation (MLE) [7–9], singular-value decomposition (SVD) [10], linear and nonlinear least squares [11, 12], linear and nonlinear phase-locked loop (PLL) [6, 13–27], quadrature signal generator-based frequency-locked loops (FLL) [28–33], various variants of Luenberger observer [26, 34–36] etc.

Based on the way the instantaneous phase is estimated, the above techniques can be broadly classified into two categories. In the first category, the techniques use a proportional-integral (PI) type (including various variants) low pass loop filter to estimate the frequency. Then by taking the time-integration of the angular frequency, the instantaneous phase is estimated. In the second category, the phase is estimated directly, by using quadratic signals through arctangent function. Since low-pass filter introduces delay, the transient response of techniques that use PI-type loop filter can be slow. The transient response can be made arbitrarily fast, however, that generally gives second-order type response in the case of frequency jump. That is why in this work, we focus on techniques that use direct phase estimation from the fast transient response perspective.

As mentioned above, some of the direct phase estimation techniques are: linear and nonlinear harmonics oscillators (including various variants) [28, 31, 33], various variants of Luenberger observer [34–36] etc. These techniques works by generating quadrature signals from the measured grid voltage. Out of these techniques, Luenberger observer type techniques recently became very popular. From the theoretical point of view, they can provide global asymp-

*Corresponding author
Email address: hafiz.h.ahmed@ieee.org (Hafiz Ahmed)

Nomenclature

$\Delta\omega$	Frequency deviation from the nominal value	A, C	State and output matrix
η, ζ	State vector x in the transformed coordinates	J	Jacobian matrix
Γ	FLL gain of SOGI-FLL	K, L	Observer gain matrices
$\hat{.}, \tilde{.}$	Estimated value and estimation error	M	Amplitude of grid voltage signal
κ	Unknown grid frequency coefficient	q	90° phase-shifting operator
$\mathcal{T}, \mathcal{B}$	Non-singular coordinate transformation matrices	V^{+}_{abc}	Positive-sequence of V_{abc}
ω, ω_n	Actual and nominal frequency of grid voltage	V^{-}_{abc}	Negative-sequence of V_{abc}
diag	Diagonal matrix	V^{0}_{abc}	Zero-sequence of V_{abc}
φ,θ	Phase and instantaneous phase of grid voltage	x	State vector of grid voltage dynamics
$\vec{V}$	Phasor notation of V_{abc}	y	Single-phase grid voltage signal

totic stability unlike oscillator based techniques. From the practical point of view, they provide fast and accurate estimation of grid voltage parameters. However, they do not employ any gain normalization in their frequency identification loop. This can be problematic in the presence of large voltage sag (e.g. 50% dip). Many grid codes around the world compels the renewable energy sources to be connected to the grid even when the grid voltage drops well beyond the nominal operating limit. This is commonly known as low-voltage-ride-through (LVRT) capability. In the low voltage context, if no gain normalization is employed in the frequency estimation block, the settling time will be significantly higher than that of nominal voltage condition (*cf.* Sec. 2 for a motivating example). This motivates the current work. In this work, we propose a novel gain normalized - frequency locked loop in the adaptive observer framework. Thanks to the gain normalization, the proposed observer converges much faster than observer that doesn't use gain normalization. In addition, we also propose the fast detection of the symmetrical components of three-phase systems using the developed observer. These are the main contributions of this paper.

The rest of the paper is organized as follows: Sec. 2 gives a motivating example to explain the idea behind the proposed work while Sec. 3 describes in the detail the proposed approach. Extension of the proposed observer for three-phase sequence detection is given in Sec. 4. Experimental results are given in Sec. 5 and finally, Sec. 6 concludes this paper.

2. Motivating Example

Let us consider the grid voltage signal given by

$$y = M \sin \underbrace{(\omega t + \varphi)}_{\theta} \tag{1}$$

where amplitude, angular frequency and phase are given by M, ω and θ respectively. If we consider $y = x_1$ and $\dot{y} = x_2 = M\omega\cos(\theta)$, then the dynamics of the grid voltage signal in the state-space form can be written as:

$$\dot{x} = \bar{A}x \tag{2}$$

$$y = \bar{C}x \tag{3}$$

where $\bar{A} = \begin{bmatrix} 0 & 1 \\ -\omega^2 & 0 \end{bmatrix}$, and $\bar{C} = \begin{bmatrix} 1 & 0 \end{bmatrix}$. Since the frequency ω is unknown with a known nominal value $\omega_n = 100\pi$ or 120π, the unknown frequency can be represented as $\omega = \sqrt{\kappa}\omega_n$ with $\kappa = \omega^2/\omega_n^2$. To estimate the parameters of system (2) -(3), several adaptive observer based solution has been recently proposed in the literature [26, 34–36]. Most of them use non-singular transformation to facilitate the adaptive observer design. As a representative example, let us consider the following non-singular transformation [35]:

$$\eta = \begin{bmatrix} \eta_1 & \eta_2 \end{bmatrix}^T = \mathcal{T}x \tag{4}$$

where $\mathcal{T} = \begin{bmatrix} \omega_n\beta_1 & -\beta_2 \\ \omega_n^2\kappa\beta_2 & \omega_n\beta_2 \end{bmatrix} / \left(\omega_n^3\beta_1^2 + \omega_n^3\kappa\beta_2^2\right), \beta_1 > 0$ and $\beta_2 > 0$ are tuning parameters. In $\eta-$ coordinate, system (2) -(3) can be written as:

$$\dot{\eta} = A\eta \tag{5}$$

$$y = C\eta \tag{6}$$

where $A = \mathcal{T}\bar{A}\mathcal{T}^{-1} = \bar{A}$ and $C = \bar{C}\mathcal{T}^{-1} = \begin{bmatrix} \omega_n^2 & \omega_n \end{bmatrix}$. For system (5) -(6), the following frequency adaptive Luenberger observer has been designed in [35]:

$$\dot{\hat{\eta}} = \hat{A}\hat{\eta} - K\left(y - C\hat{\eta}\right) \tag{7}$$

$$\dot{\kappa} = -\gamma\omega_n^2\hat{\eta}_1\left(y - C\hat{\eta}\right) \tag{8}$$

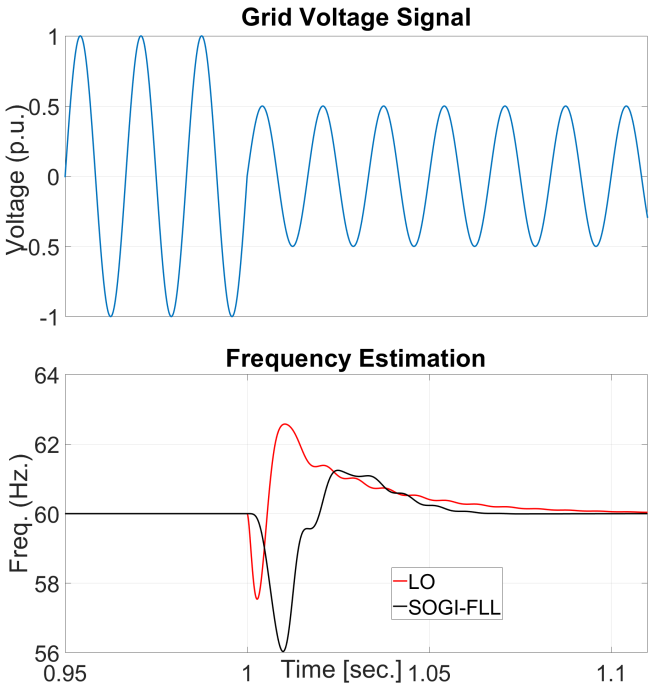

Figure 1: Simulation results for the motivating example.

where $\hat{}$ represents the estimated value and the observer gain, $K = \left[-(\omega_n\beta_2)^{-1} \; -K_2\right]^T, K_2 > 0$ and $\gamma > 0$ is the frequency estimation tuning parameter. The frequency identification part given in Eq. (8) resembles the frequency-locked loop (FLL) proposed in [28]. The FLL of [28] is obtained using special frequency domain property of the quadrature axis signal and the estimation error. The FLL (8) on the other hand is obtained with the help of Lyapunov function given in [35]. It is to be noted here that unlike [28], Eq. (8) doesn't employ any gain normalization i.e. using the estimated amplitude of the signal to normalize the right-hand side of Eq. (8). As such any grid synchronization algorithm that employs the above adaptive observer may take more time to converge in the presence of voltage sag. Moreover as low-voltage-ride-through (LVRT) capability is a desired (or compulsory, depending the local regulations) property of any grid synchronization control algorithm, this issue needs to be addressed. To illustrate this fact, let us consider a simulation study with 50% voltage sag. Parameters of the Luenberger Observer (7)-(8) are selected as $K = -[0.0027\ 1.2]^T, \gamma = 0.05$ As a comparison tool, we have selected gain normalized SOGI-FLL with parameters as $k = \sqrt{2}$ and $\Gamma = 50$. Simulation result is given in Fig. 1. By considering ± 0.1Hz. band, SOGI-FLL took $\approx$ 55msec. to converge while LO took $\approx$ 84msec. This example clearly demonstrates the effect of gain normalization and thus motivates the current work of developing gain normalized adaptive observer. Details of the proposed development is given in the following Section.

3. Gain Normalized Adaptive Observer

In this Section, we use the same dynamic model (2) -(3) as given in Sec. 2. However, to introduce gain normalization in the frequency estimation part, let us assume that the unknown frequency is represented by $\omega = \omega_n + \Delta\omega$ where $\Delta\omega$ represents the deviation from the nominal frequency. With respect to the new representation of the unknown frequency, let us consider the following non singular transformation

$$\zeta = \mathcal{B}x \tag{9}$$

where $\mathcal{B} = \begin{matrix} \omega & -1 \\ \omega^2 & \omega \end{matrix} \; / \; 2\omega^3$. In the $\zeta-$coordinate, system (2) -(3) can be written as:

$$\dot{\zeta} = A\zeta \tag{10}$$
$$y = C\zeta \tag{11}$$

where $A = \mathcal{B}\bar{A}\mathcal{B}^{-1} = \bar{A}$ and $C = \bar{C}\mathcal{B}^{-1} = [\omega^2 \; \omega]$. For system (10) -(11), the following gain normalized adaptive observer - frequency-locked loop (GN-FLL) is proposed:

$$\dot{\hat{\zeta}} = \hat{A}\hat{\zeta} + L\left(y - \hat{C}\hat{\zeta}\right) \tag{12}$$
$$\dot{\Delta\omega} = -\frac{\lambda(l_1 + l_2)\hat{\omega}^3\hat{\zeta}_1\left(y - \hat{C}\hat{\eta}\right)}{\sqrt{\frac{\left(\hat{\zeta}_1 2\hat{\omega}^3\right)^2 + \left(\hat{\zeta}_2 2\hat{\omega}^2\right)^2}{2\hat{\omega}^2}}} \tag{13}$$

where $\hat{}$ represents the estimated value, $L = [l_1\ l_2]^T$ is the observer gain and $\lambda > 0$ is the frequency identification gain.

Remark 1. During the estimation process, the states $\hat{\zeta}_1$, and $\hat{\zeta}_2$ may become zero. This will lead to a division by zero situation in (13). To overcome this issue, the denominator of (13) has been implemented as

$$\sqrt{\max\left(\frac{\left(\hat{\zeta}_1 2\hat{\omega}^3\right)^2 + \left(\hat{\zeta}_2 2\hat{\omega}^2\right)^2}{2\hat{\omega}^2}, \varepsilon\right)}$$

where $\epsilon > 0$ is a very small positive constant.

From the estimated states $\hat{\zeta}$, the state variables in the $x-$ coordinate can be obtained using the following relationship:

$$\hat{x} = \underbrace{\begin{matrix} \hat{\omega}^2 & \hat{\omega} \\ -\hat{\omega}^3 & \hat{\omega}^2 \end{matrix}}_{\hat{\mathcal{B}}^{-1}} \hat{\zeta} \tag{14}$$

From the estimated states, the instantaneous phase θ can be estimated as:

$$\hat{\theta} = \arctan\left(\hat{\omega}\hat{x}_1/\hat{x}_2\right) \tag{15}$$

A major difference between the Luenberger observer and the proposed GN-FLL is that GN-FLL uses the estimate amplitude of the signal in the right-hand side of the FLL equation (13). To check this fact, i.e. the denominator of Eq. (13) represents the amplitude, let us consider the steady-state case i.e. $\hat{\omega} = \omega_n$. In that case,

$$\zeta = \mathcal{B}x \tag{16}$$

$$\begin{matrix}\zeta_1 \\ \zeta_2\end{matrix} = \frac{1}{2\omega^3}\begin{matrix}\omega & -1 & M\sin(\theta) \\ \omega^2 & \omega & M\omega\cos(\theta)\end{matrix} \tag{17}$$

$$\begin{matrix}\zeta_1 \\ \zeta_2\end{matrix} = \frac{1}{2\omega^2}\begin{matrix}M\sin(\theta) - M\cos(\theta) \\ \omega\left\{M\sin(\theta) + M\cos(\theta)\right\}\end{matrix} \tag{18}$$

$$\begin{matrix}\zeta_1 \\ \zeta_2\end{matrix} = \frac{1}{2\omega^2}\begin{matrix}x_1 - x_2/\omega \\ x_1\omega + x_2\end{matrix} \tag{19}$$

Using the values of ζ_1 and ζ_2 given in Eq. (18)-(19) , the denominator of Eq. (13) can be written as:

$$\frac{\sqrt{\hat{\zeta}_1 2\hat{\omega}^3{}^2 + \hat{\zeta}_2 2\hat{\omega}^2{}^2}}{2\omega^2} \tag{20}$$

$$= \sqrt{\frac{\left(x_1\omega - x_2\right)^2 + \left(x_1\omega + x_2\right)^2}{2\omega^2}} \tag{21}$$

$$= \sqrt{\frac{2x_1^2\omega^2 + 2x_2^2}{2\omega^2}} \tag{22}$$

$$= \sqrt{M^2\sin^2(\omega t) + M^2\cos^2(\omega t)} \tag{23}$$

$$= M \tag{24}$$

The above calculations show the gain normalization property of the proposed GN-FLL unlike the existing Luenberger observers that use the same dynamical model (2) -(3).

3.1. Stability analysis of GN-FLL

To analyze the stability of the proposed GN-FLL, we use the linearization based approach. Before further development, let us define the observation error as, $\tilde{\zeta} = \zeta - \hat{\zeta}$. Then the dynamics of the observation error is given as

$$\dot{\tilde{\zeta}} = \dot{\zeta} - \dot{\hat{\zeta}} \tag{25}$$

$$= A\zeta - \left\{\hat{A}\hat{\zeta} + L \quad y - \hat{C}\hat{\zeta}\right)\right\} \tag{26}$$

$$\dot{\tilde{\zeta}} = (A - LC)\,\tilde{\zeta} + \left\{\left(A - \hat{A} \quad - L \quad C - \hat{C}\right\} \;\hat{\zeta} \tag{27}$$

Similarly, the FLL dynamics (13) in terms of observation error $\tilde{\zeta}$ can be written as:

$$\dot{\Delta\omega} = \frac{-\lambda(l_1 + l_2)\hat{\omega}^3\hat{\zeta}_1\left\{C\tilde{\zeta} + \quad C - \hat{C} \quad \hat{\zeta}\right\}}{\sqrt{\frac{\left(\hat{\zeta}_1 2\hat{\omega}^3\right)^2 + \left(\hat{\zeta}_2 2\hat{\omega}^2\right)^2}{2\hat{\omega}^2}}} \tag{28}$$

Table 1: Routh-Hurwitz table for polynomial (32).

s^2	1	$\omega_n^2(l_2 + 1 - l_1\omega_n)$
s^1	$l_1\omega_n^2 + l_2\omega_n$	0
s^0	$\omega_n^2(l_2 + 1 - l_1\omega_n)$	0

Closed loop error dynamics of the GN-FLL is given by (27)-(28). Near the nominal operating condition, the equilibrium point is given by:

$$\left\{\tilde{\zeta}, \Delta\omega\right\}^\star = \left\{\tilde{\zeta} = 0, \Delta\omega = 0\right\} \tag{29}$$

The Jacobian matrix of the closed-loop error dynamics of the GN-FLL evaluated at the desired equilibrium is given by:

$$J\left\{\tilde{\zeta}, \Delta\omega\right\}^\star = \begin{bmatrix} -l_1\omega_n^2 & 1 - l_1\omega_n & l_1 \\ -\omega_n^2\,(l_2 + 1) & -l_2\omega & l_2 \\ 0 & 0 & 0 \end{bmatrix} \tag{30}$$

To determine the stability of the Jacobian matrix, let us consider the characteristics polynomial of (30) given below:

$$s^3 + (l_1\omega_n^2 + l_2\omega_n)s^2 + \omega_n^2(l_2 + 1 - l_1\omega_n)s = 0 \tag{31}$$

If the elements of the gain Matrix L are selected in a way such that $l_2 + 1 \geq l_1\omega_n$, then all the coefficients of polynomial (31) are non-negative. The stability of the polynomial (31) can be obtained through Routh-Hurwitz test. For this purpose, polynomial (31) can be rewritten as:

$$s^2 + (l_1\omega_n^2 + l_2\omega_n)s + \omega_n^2(l_2 + 1 - l_1\omega_n) = 0 \tag{32}$$

To show that the polynomial (32) does not have any roots in the right-half plane, let us consider the Routh-Hurwitz table given in Table 1. From Table 1, it can be seen that if $l_2 + 1 \geq l_1\omega_n$, all the elements in the first column of the Routh-Hurwitz table are positive. This implies no sign change, as a result, no roots lie in the right-half plane. This together with the root at origin implies marginal stability of the closed-loop system. As such, the local stability of the GN-FLL can be established.

3.2. Gain tuning of GN-FLL

Proposed GN-FLL has two parameters to tune, gain matrix, L and the frequency estimation parameter λ. To tune the gain matrix L, pole placement can be the solution. Let us assume that the desired closed-loop poles are p_1 and p_2. Then the elements of L can be calculated using the following formula:

$$(s - p_1)(s - p_2) = \det\left\{sI_2 - (A - LC)\right\} \tag{33}$$

By equating the coefficients on both side of the polynomial (33), the following formulas can be obtained for gain elements:

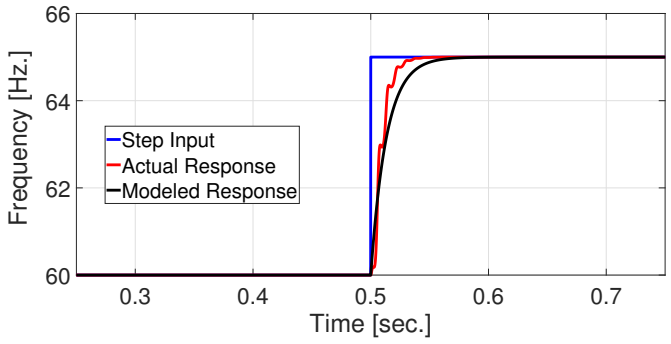

Figure 2: Frequency step-response.

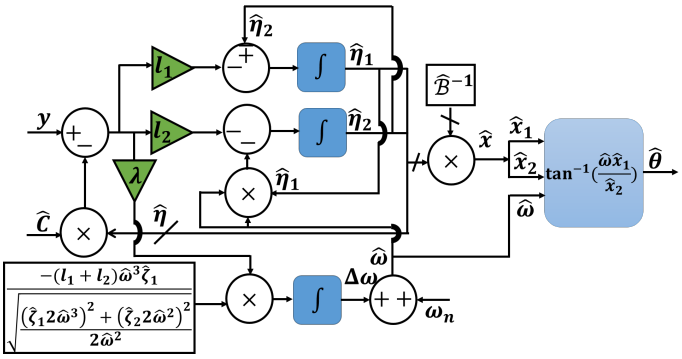

Figure 3: Block diagram of the proposed GN-FLL.

$$l_1 = \frac{-(p_1p_2 + p_1\omega_n + p_2\omega_n - \omega_n^2)}{2\omega_n^3} \tag{34}$$

$$l_2 = \frac{-(p_1\omega_n - p_1p_2 + p_2\omega_n + \omega_n^2)}{2\omega_n^2} \tag{35}$$

Tuning the parameter λ is complicated since the FLL dynamics (13) is nonlinear. In order to use the tools from linear control system, one solution is to approximate the FLL dynamics. For that purpose, we have performed a frequency step test to obtain the approximated linear system. From the step-response, it could be found that the following linear system can be used to approximate the frequency dynamics:

$$G_f(s) = \frac{\lambda\omega_n}{s + \lambda\omega_n} \tag{36}$$

For the value of $\lambda = 0.2$, the response of the FLL and the model (36) is given in Fig. (2). Since $\lambda = 0.2$ gives a close enough (sufficient for gain tuning) approximation of the nonlinear dynamics of the FLL, this value has been considered all throughout this work. It is to be noted here that eq. (36) represents a first-order approximation of the highly nonlinear FLL dynamics. As such modeling error is inevitable. However, the objective here is to simplify the gain tuning, not stability analysis. As such, any modeling error introduced by eq. (36) has no impact on the stability of the proposed GN-FLL. FLL dynamics is heavily influenced by λ. through extensive simulation study, we found that $0 < \lambda < 1$ can be considered as a good range for λ.

The proposed gain normalized adaptive observer has two parts. The first part generates quadrature signal from the measured grid voltage. In addition, a filtered copy of the grid voltage signal is also generated. In the second part, a frequency locked-loop (FLL) is used to estimate the unknown frequency of the grid voltage signal. FLL part exploits special phase relationship between the output (i.e. in-phase) estimation error and the quadrature-phase signal. In the presence of large voltage sag, the output estimation error can be significantly small. This will slow down the unknown frequency estimation dynamics. To overcome this problem, a gain normalization procedure is used. Gain normalization procedure uses the estimated amplitude in the frequency estimation dynamics similar to per unit measurement typically used in power system calculation. This significantly enhances the dynamics of the frequency estimation loop despite large voltage sag.

To implement the proposed GN-FLL, Eq. (12), (13), (14) and (15) are required. Block diagram representation is given in Fig. 3.

4. GN-FLL for Three-Phase Applications

The proposed GN-FLL can be applied to extract the symmetrical components of three-phase systems. For this purpose, let us consider the unbalanced three-phase grid voltage

$$V_{abc} = V^+_{abc} + V^-_{abc} + V^0_{abc} \tag{37}$$

where the positive, negative and zero sequence voltages are given by:

$$V^+_{abc} = v^+_{abc} \sin\left\{\omega t + \varphi^+ - \frac{2\pi k}{3}\right\} \tag{38}$$

$$V^-_{abc} = v^-_{abc} \sin\left\{\omega t + \varphi^- + \frac{2\pi k}{3}\right\} \tag{39}$$

$$V^0_{abc} = v^0_{abc} \sin\left\{\omega t + \varphi^0\right\} \tag{40}$$

where $k = 0, 1, 2$ for individual phases. Then the symmetrical components can be extracted using the following relationship [37]:

$$V^+_{abc} = T_2 V_{abc} + T_1 q V_{abc} \tag{41}$$

$$V^-_{abc} = T_2 V_{abc} - T_1 q V_{abc} \tag{42}$$

$$V^0_{abc} = \{\mathrm{diag}\,(1,1,1) - 2T_2\}\, V_{abc} \tag{43}$$

where $\mathrm{diag}\,(1,1,1)$ represents the 3×3 diagonal matrix with diagonal elements being 1, $q = e^{-j\pi/2}$ is 90° phase-shifting operator and the matrices T_1 and T_2 are given as:

$$T_1 = \frac{1}{2\sqrt{3}} \begin{bmatrix} 0 & 1 & -1 \\ -1 & 0 & 1 \\ 1 & -1 & 0 \end{bmatrix}, T_2 = \frac{1}{6} \begin{bmatrix} 2 & -1 & -1 \\ -1 & 2 & -1 \\ -1 & -1 & 2 \end{bmatrix} \tag{44}$$

GN-FLL generates quadrature signals, GN-FLL can be easily applied to estimate the symmetrical components using Eq. (41)-(43). As the system has only one frequency to estimate, so only one FLL is needed.

4.1. GN-FLL vs Luenberger observer : a comparison

The proposed GN-FLL is motivated by Luenberger type observer-based approach [34–36]. Existing Luenberger observers do not employ any gain normalization scheme. This can be problematic in the presence of large voltage sag/swell. According to grid codes, many countries now demand grid connected converters (GCC) to have low voltage ride through capability (LVRT). In this context, any controller for GCC should be able to function during large voltage sag. If gain normalization procedure is not included inside the PLL/FLL block of the controller, the controller will take much longer to stabilize. This is not desirable. As such, in this paper, we propose GN-FLL inspired by Luenberger observer. Existing Luenberger observers are designed either for single-phase [35, 36] or three-phase [34]. The proposed GN-FLL can be easily applied to single and three-phase cases. In the three-phase case, the same single-phase structure case can be applied. Only few additional transformations need to be used. This clearly distinguishes the proposed technique w.r.t. existing Luenberger observer-based techniques. Moreover, we have provided constructive rules for gain tuning using small-signal modeling. This is another contribution of the proposed work.

5. Results And Discussions

5.1. Simulation Results

5.1.1. Single-Phase

To demonstrate the suitability of the theoretical developments proposed in Sec. 3 and 4, numerical simulation studies are considered here. For the simulation study, a sampling frequency of 10kHz is considered with the nominal frequency being $\omega_n = 120\pi$. As a comparison tool, we have selected the Luenberger observer (LO) as described in Sec. 2, SOGI-PLL [19] and EPLL [18]. All the selected techniques work by generating quadrature signals (QSG). In actual grid voltage signal, various abnormalities are present e.g. sub-harmonics (SH), inter-harmonics (IH) and DC bias. The selected techniques do not consider these disturbances explicitly. In this Section, robustness of the selected techniques will be considered. To make the article concise and easy to read, standard tests i.e. frequency and amplitude step change, voltage sag etc. will be considered in Sec. 5.2 through experimental study.

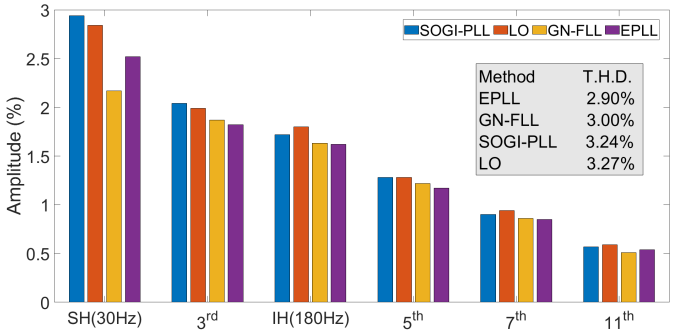

Figure 4: Harmonic distortion results of simulation harmonics test.

5.1.2. Harmonics test

In this test, harmonics are suddenly added to the grid voltage signal. The selected harmonics signal comprised of 3^{rd},5^{th},7^{th} and 11^{th} order harmonics, sub-harmonics of 30Hz and inter-harmonics of 180Hz, with each having an amplitude of 0.03p.u. This implies a total harmonic distortion (THD) of 7.35%. Harmonic distortion generated by the selected techniques for this test is given in Fig. 4 while the estimated phase and frequency are given in Fig. 6 (a). From the THD results of Fig. 4, it can be seen that the proposed GN-FLL has very good harmonic filtering capability. It has a THD of 3.00% while SOGI-PLL and LO has a THD of 3.24% and 3.27%, respectively. This results in $\approx$ 60% reduction in harmonics for GN-FLL while $\approx$ 55% for LO and SOGI-PLL. The proposed GN-FLL does not use any loop-filters unlike EPLL and SOGI-PLL, yet the THD of GN-FLL is almost identical to EPLL which is the best performing technique in terms of THD. Moreover, GN-FLL produced significantly less distortion with respect to sub-harmonics. This property is very important if we want to use it inside any grid-connected converter controller. In today's power system, the contribution of LED lighting and various other non-linear loads are increasing. As such the contribution of sub-harmonics and inter-harmonics are increasing. There are many techniques available in the literature to filter out odd-harmonics. However, filtering out sub-harmonics and inter-harmonics are not straightforward. GN-FLL can be very useful in this regard. In term of frequency estimation, GN-FLL has better performance w.r.t. other techniques while the phase estimation error of GN-FLL is similar to EPLL and LO. Fig. 4 and 6(a) show that the proposed GN-FLL has very good filtering property.

5.1.3. DC bias test

In this test, DC bias of 0.2p.u. has suddenly been added to the grid voltage. Controllers for grid-connected inverters are implemented in general in micro-controller, DSP, etc. The feedback of the grid voltage signal is obtained through an analog-to-digital converter (ADC). This process may add measurement offset. Moreover, DC offset may appear as a result of fault or transformer saturation.

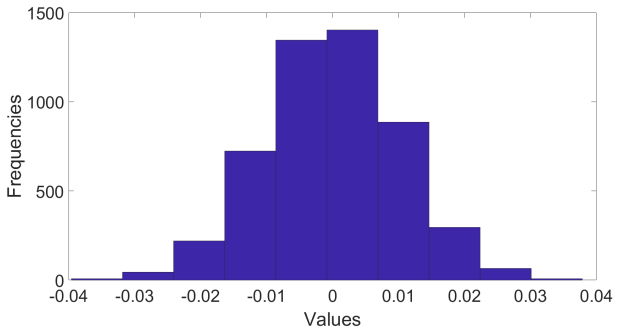

Figure 5: Histogram of noise distributions.

As such it may not be avoided in real-life. This test considers the challenging situation involving DC offset. Simulation results are given in Fig. 6(b). Fig.6(b). shows that the proposed GN-FLL and EPLL have very good performance in terms of frequency estimation w.r.t. LO and SOGI-PLL. The ripple magnitude for GN and EPLL are bounded within a range of 3Hz while SOGI-PLL and LO have significantly higher ripple magnitude. However, in term of phase estimation, SOGI-PLL performed slightly better than that of the GN-FLL where as EPLL and LO performed not so good. The ripple magnitude of GN-FLL and SOGI-PLL are almost half of EPLL and LO. This test demonstrates that the proposed GN-FLL can be useful despite the presence of large amplitude DC bias in the grid voltage signal.

5.1.4. Noise test

In this test, Gaussian measurement noise (zero mean and variance 10^{-4}) is suddenly added to the grid voltage signal. Histogram plot of the noise signal is given in Fig. 5. Simulation results are given in Fig. 6(c). From the estimated frequency in Fig. 6(c), it can be seen that GN-FLL and EPLL performs significantly better than LO and SOGI-PLL. The frequency estimated by GN-FLL and EPLL has the ripple bounded by ± 0.05Hz while for SOGI-PLL and LO, the ripple magnitude is more than two times than that of other techniques. In term of phase estimation error, SOGI-PLL showed better performance, however, GN-FLL showed better performance w.r.t. EPLL and LO. GN-FLL's ripple magnitude is slightly higher than that of the best performing technique SOGI-PLL. If we consider both frequency and phase estimation, GN-FLL can be considered as the overall best technique.

5.1.5. Three-phase

All the selected techniques in Sec. 5.1 work by generating quadrature signals. However, there are other non-QSG based PLL techniques available in the literature e.g. non-adaptive moving average filter (NMAF)-PLL (NMAF-PLL) [38], Clarke transformation-based discrete Fourier transform (CT-DFT) [39]. It is to be noted here that the purpose of GN-FLL for three-phase case is to estimate sequences. CT-DFT and NMAF-PLL are more suitable to estimate the phase and frequency. They were not designed to estimate the positive, negative, and zero sequence voltages of an unbalanced three-phase grid voltage system. Although it is to be mentioned here that through proper modification, it is possible to detect the sequences of three-phase signal through CT-DFT and NMAF-PLL. However, this is beyond the scope of the current work. In this work, our focus is on FLL/PLL type techniques, that is why NMAF-PLL is considered for further analysis.

To test the performance of GN-FLL and NMAF-PLL, an unbalanced grid voltage is considered. Before the fault, the symmetrical components are set as $\vec{V}^+ = 1\angle 0^\circ, \vec{V}^- = 0, \vec{V}^0 = 0$. After the fault, the grid became unbalanced with $\vec{V}^+ = 0.5\angle 30^\circ, \vec{V}^- = 0.3\angle -50^\circ, \vec{V}^0 = 0.2\angle 0^\circ$. Unbalance fault is not so uncommon for three-phase system. As such this test scenario is very realistic and at the same time very challenging. The results of the simulation are given in Fig. 7. Figure 7 demonstrates that despite the unbalanced fault, the frequency estimation error converged in ≈ 0.75 cycle whereas NMAF-PLL took ≈ 3 cycles. The peak overshoot for NMAF-PLL is almost 5Hz where as it is less than 0.5Hz for GN-FLL. GN-FLL doesn't involving any averaging calculation whereas NMAF-PLL does involve averaging. This will add additional computational cost w.r.t. GN-FLL. This concludes on the suitability of GN-FLL for unbalanced three-phase system.

5.2. Experimental Results

To validate the results of the proposed GN-FLL, dSPACE 1104 board based hardware-in-the-hoop (HIL) experimental studies have been considered in this Section. For the practical implementation, a sampling frequency of 10kHz is considered. Proposed GN-FLL has two parameters to tune. First to tune the observer gain, let us consider the desired closed-loop poles as $p_1 = -1.5\omega_n + j\omega_n$ and $p_2 = -1.5 - j\omega_n$ with $\omega_n = 120\pi$. Then applying the formula (34) and (35), the observer gain is found to be $L = \begin{bmatrix} 9.9472 \cdot 10^{-4} & 2.6250 \end{bmatrix}^T$. Since $l_2 + 1 > l_1\omega_n$, the stability is assured as discussed in Sec. 3.1. The frequency identification parameter is set to be $\lambda = 0.2$ as discussed in Sec. 3.2. As a comparison tool, we have selected the Luenberger observer (LO) as described in Sec. 2, SOGI-PLL [19] and EPLL [18]. The parameters of LO are selected the same as in Sec. 2, SOGI-PLL parameters are selected as: $k = 2.1$, $k_p = 137.5$ and $k_i = 7878$ according to the optimized values given in [40], the parameters of EPLL are selected as: $\mu_1 = \mu_3 = \omega_n$ and $\mu_2 = \omega_n^2/8$ according the optimized values given in [18].

To test the algorithms, the following test conditions have been considered:

1. Test - I: -0.4p.u. change in amplitude
2. Test - II: $+5$Hz. change in Frequency
3. Test - III: -45° change in Phase

(a) Harmonics test.

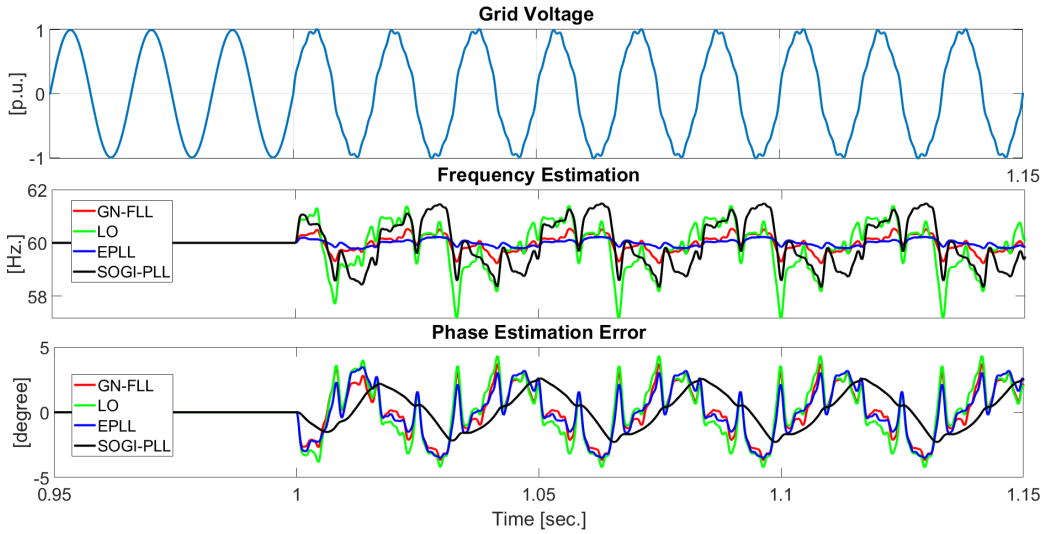

(b) DC bias test.

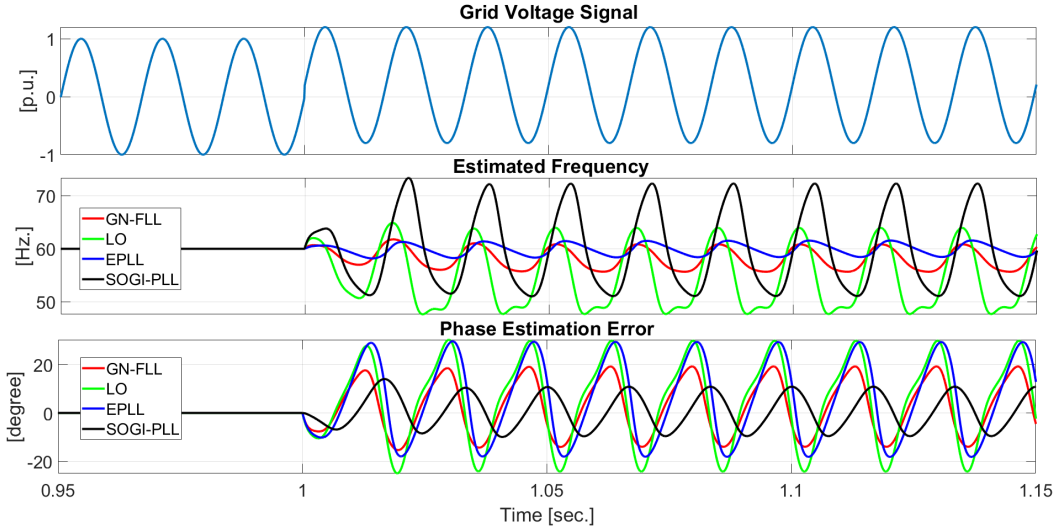

(c) Noise test.

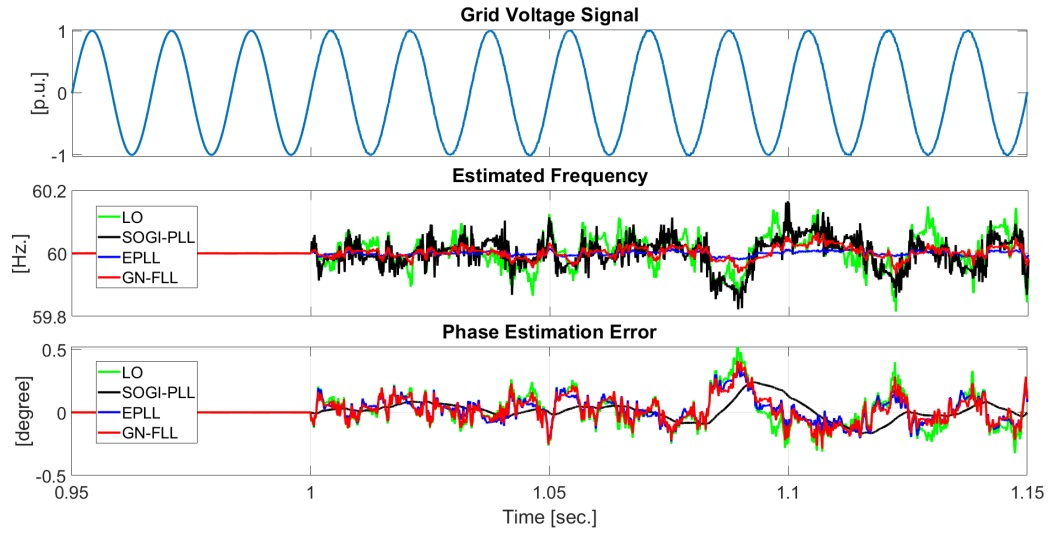

Figure 6: Simulation results for the single-phase case: (a) harmonics test, (b) DC bias test, and (c) noise test.

Table 2: Comparative time domain performance summary.

Characteristics	Test-I: Amplitude Change				Test-II: Frequency Change				Test-III: Phase Change			
	GN	LO	SOGI	EPLL	GN	LO	SOGI	EPLL	GN	LO	SOGI	EPLL
Settling time (±0.1Hz.)(ms)	30	65	55	58	28	27	46	61	32	30	53	69
Settling time (±0.1°)(ms)	5	32	58	26	12	10	35	46	19	17	44	52
Frequency overshoot (Hz.)	1.2	3	4.4	1.3	0	0	2	0	8.8	15.1	13.6	4.2
Instantaneous phase overshoot (°)	7.3	16.15	8.6	10.8	5.5	6	11.9	8.8	NA	NA	NA	NA

*GN = GN-FLL, SOGI= SOGI-PLL, NA=Not applicable, since the maximum instantaneous phase error is −45°, phase overshoot is omitted for Test-III.

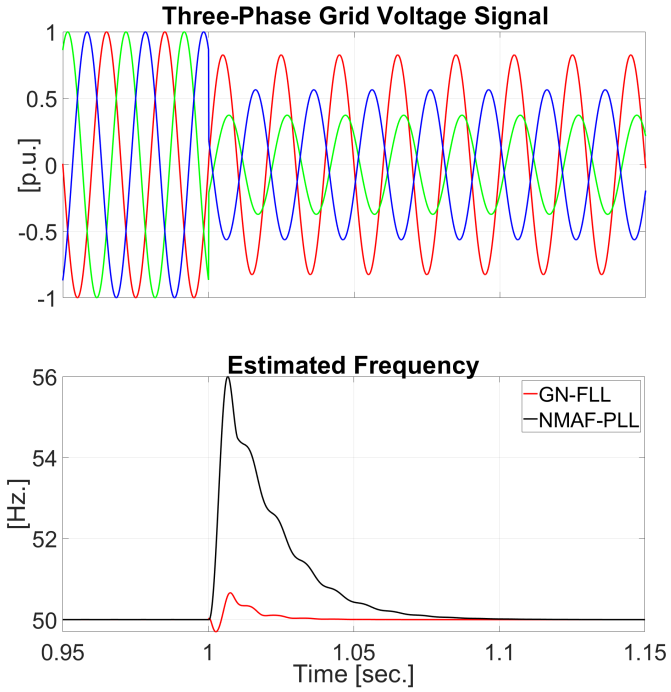

Figure 7: Simulation results for the three-phase unbalanced case.

Test-I: −0.4p.u. Change in Amplitude

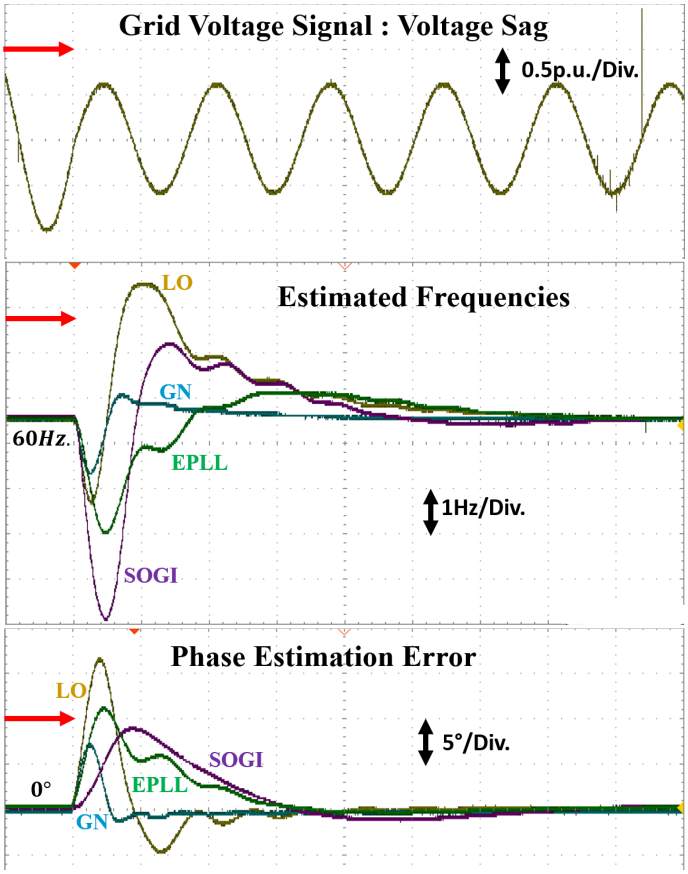

Figure 8: Experimental results for Test-I. X-axis scale: 10msec./Div.

Test-II: +5Hz. Change in Frequency

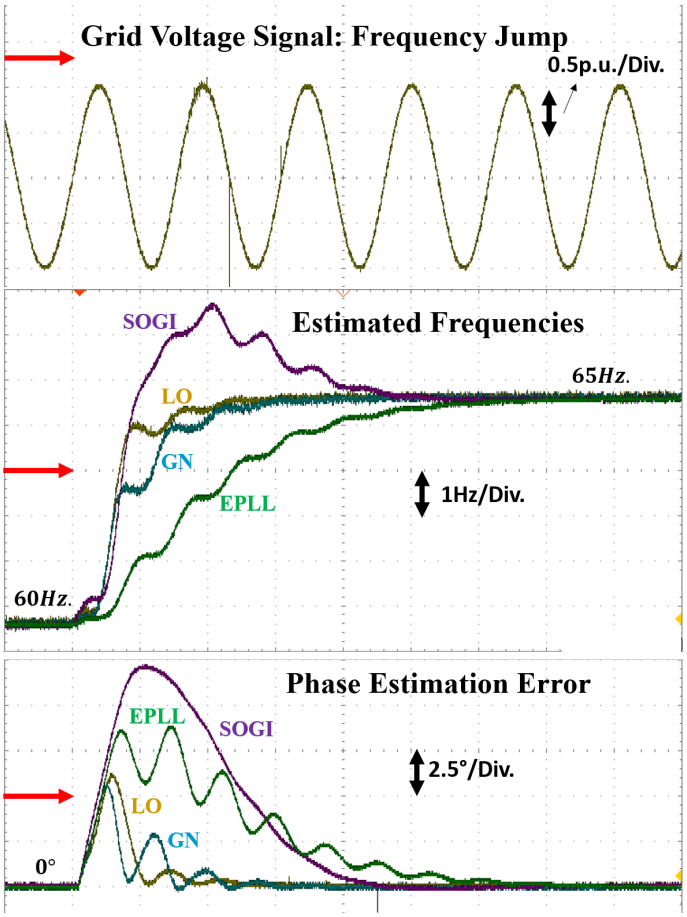

Figure 9: Experimental results for Test-II. X-axis scale: 10msec./Div.

Test-III: -45° Change in Phase

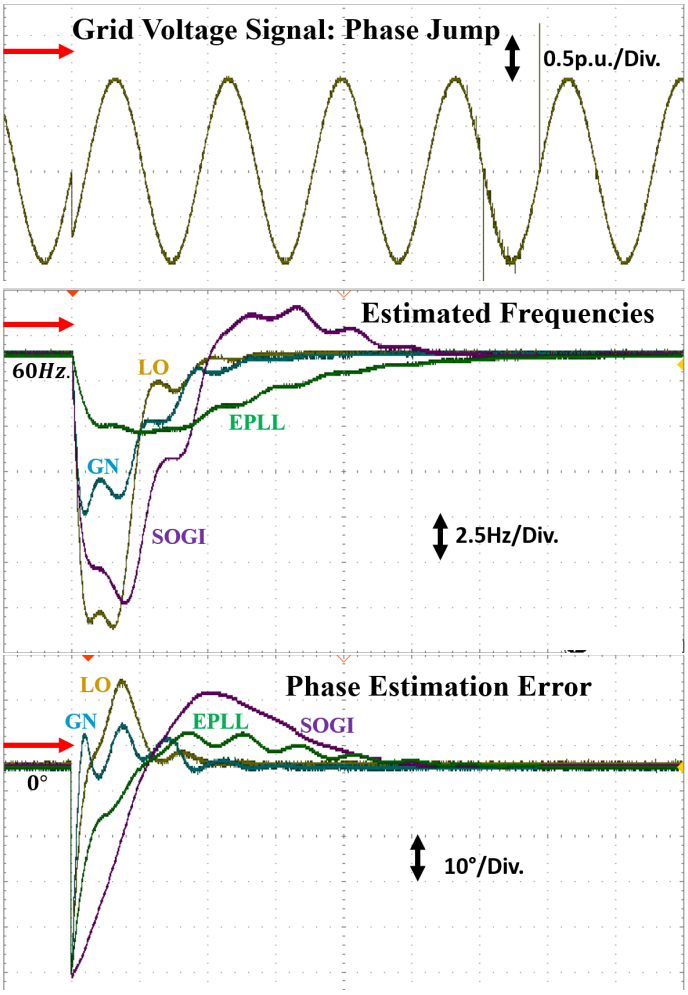

Figure 10: Experimental results for Test-III. X-axis scale: 10msec./Div.

5.3. Test - I: Amplitude Step Test

To test the performance of the algorithm in the context of low-voltage-ride-through capability situation, a step change of -0.4p.u.in amplitude is considered. Experimental results for this test scenario are given in Fig. 8. From Fig. 8, it can be seen that the proposed GN-FLL converged much faster than the other techniques. The frequency estimation error converged two times faster than the next best technique SOGI-PLL wheres phase estimation error converged 5 times faster than the next best best technique EPLL. GN-FLL also outperformed the comparative techniques in terms of peak overshoots for phase and frequency estimation error. The experimental results clearly demonstrate the benefit of the proposed GN-FLL.

5.4. Test - II: Frequency Step Test

In this test, initially the frequency of the grid voltage is set to 60Hz. Suddenly a discontinuous jump of +5Hz. is applied. Comparative experimental results are given in Fig. 9. Fig. 9 shows that in terms of frequency estimation error, GN-FLL and LO have similar convergence time where as SOGI-PLL and EPLL has much higher convergence time. Except SOGI-PLL, the other techniques converged with no peak frequency overshoot. Similar to frequency estimation error, GN-FLL and LO have similar convergence time for phase estimation error as well. However, the convergence time is more than 3 times for SOGI-PLL and EPLL. This test demonstrates the suitability of adaptive observer based technique.

5.5. Test - III: Phase Step Test

In this test, a sudden phase jump of $-45^{\circ}$is applied. Comparative experimental results for this test are given in Fig. 10. The results are very similar to the other test cases. GN-FLL and LO have similar performances while SOGI-PLL and EPLL have slower responses than that of the adaptive observer based techniques. One point to note here that although the convergence time is very similar for GN-FLL and LO, however, the peak frequency overshoot is two times more for LO with respect to GN-FLL. This is a clear indication of the effectiveness of GN-FLL.

A summary of the time domain performances in these test cases are given in Table 2. From Fig. 8, 9 and 10, the advantage of the proposed GN-FLL is very clear. GN-FLL uses gain normalization which is very useful specially in the case of voltage sag i.e. Test-I. The frequency estimation error for GN-FLL converged in $\approx$ 30msec., whereas for unnormalized Luenberger observer, it took $\approx$ 65msec. In all the test cases, GN-FLL performed similar or better than LO. It outperformed SOGI-PLL and EPLL in almost every cases. This demonstrated the effectiveness of the GN-FLL for single-phase systems.

5.6. Three-Phase Unbalanced Grid

To test the GN-FLL for the three-phase system, an unbalanced grid voltage is considered. As comparison techniques, in this Section, we have chosen double SOGI-FLL (DSOGI-FLL) [41] and adaptive notch filter (ANF) [42]. Both ANF and DSOGI-FLL are designed for unbalanced grid. The parameters of DSOGI-FLL are chose as, $k = \sqrt{2}$ and $\gamma = 50$. These values are suggested in [41]. The parameters of ANF are selected as $\gamma = 18000$ and $\zeta = 1/\sqrt{2}$ as recommended in [42].

We assume that unbalanced fault occurred in the grid. Before the fault, the symmetrical components are set as $\vec{V}^{+} = 1\angle 0^{\circ}, \vec{V}^{-} = 0$. After the fault, the grid became unbalanced with $\vec{V}^{+} = 0.75\angle -30^{\circ}, \vec{V}^{-} = 0.25\angle 110^{\circ}$. In addition, the grid frequency also changed from 60Hz. to 62Hz. Considered grid voltage and estimated frequencies by the comparative techniques for the unbalanced grid are given in Fig. 11. Moreover, the estimated positive and negative sequence voltages are given in Figs. 12 and 13. Figure 11 demonstrates that despite the unbalanced fault and the frequency jump, the frequency estimation error converged in ≈ 1.5 cycles for the proposed GN-FLL while it took ≈ 2.8 cycles for DSOGI-FLL and ≈ 4 cycles for ANF. This shows that the proposed GN-FLL is very suitable to track unknown frequencies even in unbalanced grid voltages condition. Moreover, the estimation for both positive and negative sequence components also converged very rapidly as shown in Figs. 12 and 13. This concludes the effectiveness of GN-FLL for unbalanced three-phase system w.r.t. DSOGI-FLL and ANF.

5.7. Applications to Inverter Control

In this work, we have proposed a gain normalized adaptive observer for three-phase systems. This technique can be used to extract the symmetrical components of the unbalanced grid voltage signals. This is very useful to synchronize grid connected inverters in unbalanced grid. As detailed in Sec. VI.B of [43], in the presence of unbalance fault, grid-connected converters can synchronize with the fundamental frequency positive sequence (FFPS) grid voltages. The proposed GN-FLL is capable to extract the FFPS voltages. As such GN-FLL can become an integral part of grid-connected inverter controller. The algorithm is computationally simple and easy to implement. As such, it can be easily implemented inside the existing microcontroller or DSP-based controller without any additional cost.

6. Conclusion and Future Work

This paper has proposed a novel gain normalized adaptive observer for the parameter and sequences estimation of unbalanced grid. The gain normalization helps to achieve fast convergence in the presence of large voltage sag unlike existing alternatives. Comparative experimental results demonstrated the benefit of the proposed solution.

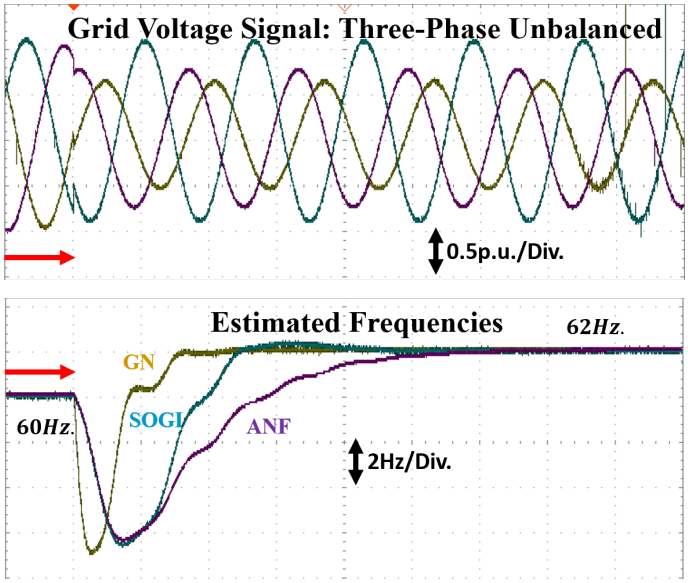

Figure 11: Experimental results for unbalanced grid with frequency step change. X-axis scale: 10msec./Div.

The main limitation of the proposed technique is it's harmonic filtering capability. Same goes for any Luenberger observer-based technique. Existing PLL-based techniques employ proportional integral (PI) controller to estimate the frequency. PI is a low-pass type filter. This adds harmonic filtering property to PLL-based technique, however, at the cost of slow dynamic response. FLL-based techniques e.g. proposed technique, estimate the frequency directly without any filtering. As a result, the fast dynamic response comes at the cost of lower harmonic filtering property. To overcome this issue, various techniques have been reported in the literature. One popular approach in this regard is to use frequency-adaptive pre-filtering technique. This will be considered in a future work. The proposed observer can only guarantee local stability i.e. in the close vicinity near the equilibrium. From the theoretical point of view, global stability is more interesting. This issue will also be considered in a future work.

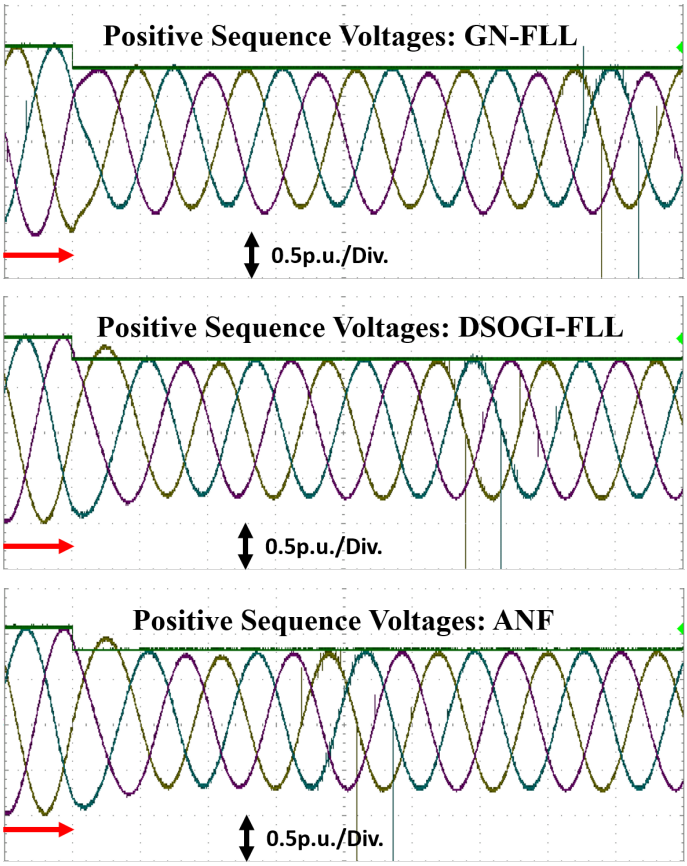

Figure 12: Estimated positive sequence voltages by various techniques. X-axis scale: 10msec./Div.

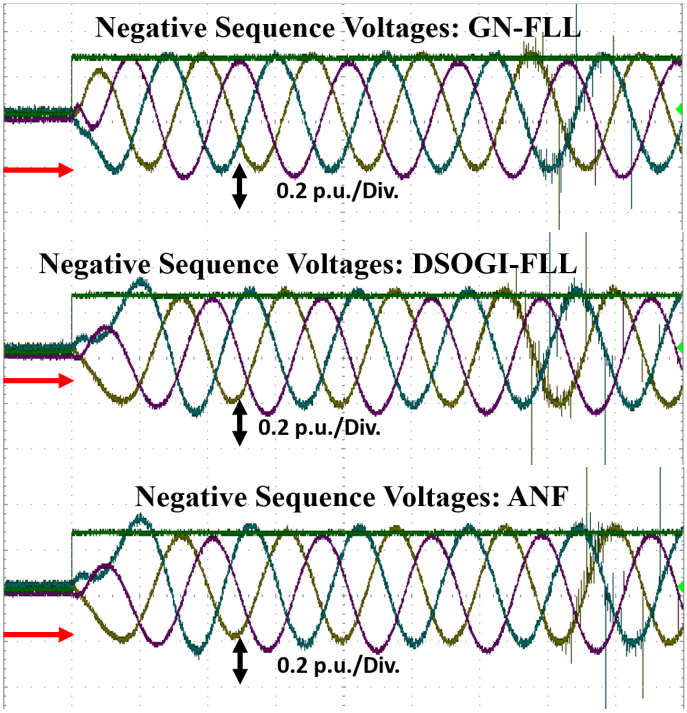

Figure 13: Estimated negative sequence voltages by various techniques. X-axis scale: 10msec./Div.

References

[1] N. Jaalam, N. Rahim, A. Bakar, C. Tan, and A. M. Haidar, "A comprehensive review of synchronization methods for grid-connected converters of renewable energy source," *Renewable and Sustainable Energy Reviews*, vol. 59, pp. 1471–1481, 2016.

[2] M. S. Almas and L. Vanfretti, "RT-HIL implementation of the hybrid synchrophasor and GOOSE-based passive islanding schemes," *IEEE Transactions on Power Delivery*, vol. 31, no. 3, pp. 1299–1309, 2015.

[3] M. Merai, W. Naouar, I. Slama-Belkhodja, and E. Monmasson, "An adaptive PI controller design for DC-link voltage control of single-phase grid-connected converters," *IEEE Transactions on Industrial Electronics*, vol. 66, no. 8, pp. 6241 – 6249, 2019.

[4] C. Cecati, F. Ciancetta, and P. Siano, "A multilevel inverter for photovoltaic systems with fuzzy logic control," *IEEE Transactions on Industrial Electronics*, vol. 57, no. 12, pp. 4115–4125, 2010.

[5] A. Safa, E. M. Berkouk, Y. Messlem, Z. Chedjara, and A. Gouichiche, "A pseudo open loop synchronization technique for heavily distorted grid voltage," *Electric Power Systems Research*, vol. 158, pp. 136–146, 2018.

[6] F. D. Freijedo, J. Doval-Gandoy, O. Lopez, C. Martinez-Penalver, A. G. Yepes, P. Fernandez-Comesana, J. Malvar, A. Nogueiras, J. Marcos, and A. Lago, "Grid-synchronization methods for power converters," in *2009 35th Annual Conference of IEEE Industrial Electronics*. IEEE, 2009, pp. 522–529.

[7] Z. Oubrahim, V. Choqueuse, Y. Amirat, and M. E. H. Benbouzid, "Maximum-likelihood frequency and phasor estimations for electric power grid monitoring," *IEEE Transactions on Industrial Informatics*, vol. 14, no. 1, pp. 167–177, 2018.

[8] V. Choqueuse, A. Belouchrani, F. Auger, and M. Benbouzid, "Frequency and phasor estimations in three-phase systems: Maximum likelihood algorithms and theoretical performance," *IEEE Transactions on Smart Grid*, vol. 10, no. 3, pp. 3248 – 3258, 2019.

[9] V. Choqueuse, A. Belouchrani, E.-H. El Bouchikhi, and M. E. H. Benbouzid, "Estimation of amplitude, phase and unbalance parameters in three-phase systems: Analytical solutions, efficient implementation and performance analysis," *IEEE Transactions on Signal Processing*, vol. 62, no. 16, pp. 4064–4076, 2014.

[10] V. Choqueuse, P. Granjon, A. Belouchrani, F. Auger, and M. Benbouzid, "Monitoring of three-phase signals based on singular-value decomposition," *IEEE Transactions on Smart Grid*, 2019.

[11] A. Vidal, F. D. Freijedo, A. G. Yepes, P. Fernandez-Comesaña, J. Malvar, O. Lopez, and J. Doval-Gandoy, "A fast, accurate and robust algorithm to detect fundamental and harmonic sequences," in *2010 IEEE Energy Conversion Congress and Exposition*. IEEE, 2010, pp. 1047–1052.

[12] Y. Terriche, J. M. Guerrero, and J. C. Vasquez, "Performance improvement of shunt active power filter based on non-linear least-square approach," *Electric Power Systems Research*, vol. 160, pp. 44–55, 2018.

[13] K. Tahir, C. Belfedal, T. Allaoui, and G. Champenois, "A new control strategy of WFSG-based wind turbine to enhance the LVRT capability," *International Journal of Electrical Power & Energy Systems*, vol. 79, pp. 172–187, 2016.

[14] F. D. Freijedo, A. G. Yepes, O. Lopez, A. Vidal, and J. Doval-Gandoy, "Three-phase PLLs with fast postfault retracking and steady-state rejection of voltage unbalance and harmonics by means of lead compensation," *IEEE Transactions on Power Electronics*, vol. 26, no. 1, pp. 85–97, 2011.

[15] B. I. Rani, C. Aravind, G. S. Ilango, and C. Nagamani, "A three phase PLL with a dynamic feed forward frequency estimator for synchronization of grid connected converters under wide frequency variations," *International Journal of Electrical Power & Energy Systems*, vol. 41, no. 1, pp. 63–70, 2012.

[16] A. Safa, E. M. Berkouk, Y. Messlem, and A. Gouichiche, "A robust control algorithm for a multifunctional grid tied inverter to enhance the power quality of a microgrid under unbalanced conditions," *International Journal of Electrical Power & Energy Systems*, vol. 100, pp. 253–264, 2018.

[17] H. A. Hamed, A. F. Abdou, E. H. Bayoumi, and E. El-Kholy, "A fast recovery technique for grid-connected converters after short dips using a hybrid structure PLL," *IEEE Transactions on Industrial Electronics*, vol. 65, no. 4, pp. 3056–3068, 2018.

[18] M. Karimi-Ghartema, *Enhanced phase-locked loop structures for power and energy applications*. John Wiley & Sons, 2014.

[19] M. Ciobotaru, R. Teodorescu, and F. Blaabjerg, "A new single-phase PLL structure based on second order generalized integrator," in *Power Electronics Specialists Conference, 2006. PESC'06. 37th IEEE*. IEEE, 2006, pp. 1–6.

[20] I. Carugati, P. Donato, S. Maestri, D. Carrica, and M. Benedetti, "Frequency adaptive PLL for polluted single-phase grids," *IEEE Transactions on Power Electronics*, vol. 27, no. 5, pp. 2396–2404, 2012.

[21] H. Ahmed, M. L. Pay, M. Benbouzid, Y. Amirat, and E. El-bouchikhi, "Hybrid estimator-based harmonic robust grid synchronization technique," *Electric Power Systems Research*, vol. 177, p. 106013, 2019.

[22] A. Elrayyah, Y. Sozer, and M. Elbuluk, "Robust phase locked-loop algorithm for single-phase utility-interactive inverters," *IET Power Electronics*, vol. 7, no. 5, pp. 1064–1072, 2014.

[23] H. Hamed, A. Abdou, E. Bayoumi, and E. EL-Kholy, "Effective design and implementation of GSS-PLL under voltage dip and phase interruption," *IET Power Electronics*, vol. 11, no. 6, pp. 1018–1028, 2018.

[24] A. Menadi, S. Abdeddaim, A. Ghamri, and A. Betka, "Implementation of fuzzy-sliding mode based control of a grid connected photovoltaic system," *ISA transactions*, vol. 58, pp. 586–594, 2015.

[25] D. Stojić, N. Georgijević, M. Rivera, and S. Milić, "Novel orthogonal signal generator for single phase PLL applications," *IET Power Electronics*, vol. 11, no. 3, pp. 427 – 433, 2018.

[26] M. Vekić, M. R. Rapaić, T. B. Šekara, S. Grabić, and E. Adžić, "Multi–resonant observer PLL with real-time estimation of grid unbalances," *International Journal of Electrical Power & Energy Systems*, vol. 108, pp. 52–60, 2019.

[27] H. Ahmed, M. Bierhoff, and M. Benbouzid, "Multiple nonlinear harmonic oscillator-based frequency estimation for distorted grid voltage," *IEEE Transactions on Instrumentation and Measurement*, 2019.

[28] P. Rodríguez, A. Luna, I. Candela, R. Mujal, R. Teodorescu, and F. Blaabjerg, "Multiresonant frequency-locked loop for grid synchronization of power converters under distorted grid conditions," *IEEE Transactions on Industrial Electronics*, vol. 58, no. 1, pp. 127–138, 2011.

[29] H. Ahmed, S.-A. Amamra, and M. Bierhoff, "Frequency-locked loop based estimation of single-phase grid voltage parameters," *IEEE Transactions on Industrial Electronics*, vol. 66, no. 11, pp. 8856 – 8859, 2019.

[30] M. L. Pay and H. Ahmed, "Modeling and tuning of circular limit cycle oscillator FLL with pre-loop filter," *IEEE Transactions on Industrial Electronics*, vol. 66, no. 12, pp. 9632 – 9635, 2019.

[31] P. Šimek, J. Škramlík, and V. Valouch, "A frequency locked loop strategy for synchronization of inverters used in distributed energy sources," *International Journal of Electrical Power & Energy Systems*, vol. 107, pp. 120–130, 2019.

[32] I. Ziouani, D. Boukhetala, A.-M. Darcherif, B. Amghar, and I. El Abbassi, "Hierarchical control for flexible microgrid based on three-phase voltage source inverters operated in parallel," *International Journal of Electrical Power & Energy Systems*, vol. 95, pp. 188–201, 2018.

[33] A. Kherbachi, A. Chouder, A. Bendib, K. Kara, and S. Barkat, "Enhanced structure of second-order generalized integrator frequency-locked loop suitable for DC-offset rejection in single-phase systems," *Electric Power Systems Research*, vol. 170, pp. 348–357, 2019.

[34] P. Shah and B. Singh, "Adaptive observer based control for rooftop solar PV system," *IEEE Transactions on Power Electronics*, 2019.

[35] Z. Dai, W. Lin, and H. Lin, "Estimation of single-phase grid voltage parameters with zero steady-state error," *IEEE Transactions on Power Electronics*, vol. 31, no. 5, pp. 3867–3879, 2016.

[36] H. Ahmed, S. Amamra, and I. Salgado, "Fast estimation of phase and frequency for single phase grid signal," *IEEE Transactions on Industrial Electronics*, vol. 66, no. 8, pp. 6408–6411, 2019.

[37] C. L. Fortescue, "Method of symmetrical co-ordinates applied to the solution of polyphase networks," *Transactions of the American Institute of Electrical Engineers*, vol. 37, no. 2, pp. 1027–1140, 1918.

[38] S. Golestan, J. M. Guerrero, and J. C. Vasquez, "Three-phase PLLs: A review of recent advances," *IEEE Transactions on Power Electronics*, vol. 32, no. 3, pp. 1894–1907, 2017.

[39] L. Zhan, Y. Liu, and Y. Liu, "A Clarke transformation-based DFT phasor and frequency algorithm for wide frequency range,"

IEEE Transactions on Smart Grid, vol. 9, no. 1, pp. 67–77, 2018.

[40] S. Golestan, M. Monfared, F. D. Freijedo, and J. M. Guerrero, "Dynamics assessment of advanced single-phase PLL structures," *IEEE transactions on industrial electronics*, vol. 60, no. 6, pp. 2167–2177, 2012.

[41] P. Rodriguez, A. Luna, R. S. Munoz-Aguilar, I. Etxeberria-Otadui, R. Teodorescu, and F. Blaabjerg, "A stationary reference frame grid synchronization system for three-phase grid-connected power converters under adverse grid conditions," *IEEE transactions on power electronics*, vol. 27, no. 1, pp. 99–112, 2011.

[42] D. Yazdani, M. Mojiri, A. Bakhshai, and G. Joós, "A fast and accurate synchronization technique for extraction of symmetrical components," *IEEE Transactions on Power Electronics*, vol. 24, no. 3, pp. 674–684, 2009.

[43] F. Blaabjerg, R. Teodorescu, M. Liserre, and A. V. Timbus, "Overview of control and grid synchronization for distributed power generation systems," *IEEE Transactions on industrial electronics*, vol. 53, no. 5, pp. 1398–1409, 2006.